Available online at www.sciencedirect.com
SCIENCE DIRECT®
Journal of Inorganic Biochemistry 98 (2004) 2052–2062
Journal of Inorganic Biochemistry
www.elsevier.com/locate/jinorgbio

Synthetic analogue approach to metallobleomycins: syntheses, structure and properties of mononuclear and tetranuclear gallium(III) complexes of a ligand that resembles the metal-binding site of bleomycin

Anastasia Manessi [a], Giannis S. Papaefstathiou [a], Catherine P. Raptopoulou [b], Aris Terzis [b], Theodoros F. Zafiropoulos [a,*]

[a] *Department of Chemistry, University of Patras, GR 265 04 Patras, Greece*
[b] *Institute of Materials Science, NCSR "Demokritos", GR 153 10 Aghia Paraskevi Attikis, Greece*

Received 7 June 2004; received in revised form 8 September 2004; accepted 9 September 2004
Available online 18 October 2004

Abstract

As part of our interest into the bioinorganic chemistry of gallium, gallium(III) complexes of the peptide ligand *N*-(2-(4-imidazolyl)ethyl)pyridine-2-carboxamide ($pypepH_2$) resembling a fragment of the metal-binding domain of bleomycins (BLMs), have been isolated. Reaction of $pypepH_2$ with $(Et_4N)[GaCl_4]$ and $Ga(acac)_3$ [$acac^-$ is the acetylacetonate(−1) ion] affords the mononuclear complex $[Ga(pypepH)_2]Cl \cdot 2H_2O$ (**1**) and the tetranuclear complex $[Ga_4(acac)_4(pypep)_4] \cdot 4.4H_2O$ (**2**), respectively. Both complexes were characterized by single-crystal X-ray crystallography, IR spectroscopy and thermal decomposition data. The $pypepH^-$ ion in **1** behaves as a N(pyridyl), N(deprotonated amide), N(pyridine-type imidazole) chelating ligand. The doubly deprotonated $pypep^{2-}$ ion in **2** behaves as a N(pyridyl), N(deprotonated amide), N(imidazolate), N′(imidazolate) μ_2 ligand and binds to one Ga^{III} atom at its pyridyl, amide and one of the imidazolate nitrogens, and to a second metal ion at the other imidazolate nitrogen; a chelating $acac^-$ ligand completes six coordination at each Ga^{III} centre. The IR data are discussed in terms of the nature of bonding and known structures. The ^1H NMR spectrum of **1** suggests that the cation of the complex maintains its integrity in dimethylsulfoxide (DMSO) solution. Complexes **1** and **2** are the first synthetic analogues of metallobleomycins with gallium(III).

Keywords: Gallium(III) complexes; N-(2-(4-imidazolyl)ethyl)pyridine-2-carboxamide metal complexes; Metallobleomycins; Synthetic analogues; X-ray crystal structures

1. Introduction

Bleomycins (BLMs), a family of natural occurring glycopeptide antibiotics, have a proven activity against testicular cancer, prostate, skin carcinomas, Hodgkin's lymphoma, and head and neck tumors [1,2]. The commercial form of these drugs, blenoxane, contains ca. 70% bleomycin A_2, 25% bleomycin B_2, and trace amounts of other congeners. The antitumor activity of BLM is attributed to its ability to cleave single- and double-stranded DNA [3–5]; more recently, it was postulated that BLM can also cleave various types of RNA [6]. The structure of BLM, as exemplified by one member of this family (BLM A_2, Scheme 1), can be subdivided into three domains: the metal-binding domain, the bithiazole moiety with a positively charged alkyl substituent attached to it, and a disaccharide unit. Although the metal-binding domain is held responsible

* Corresponding author. Tel./fax: +30 2610 997139.
E-mail address: tzafir@chemistry.upatras.gr (T.F. Zafiropoulos).

0162-0134/$ - see front matter © 2004 Elsevier Inc. All rights reserved.
doi:10.1016/j.jinorgbio.2004.09.009

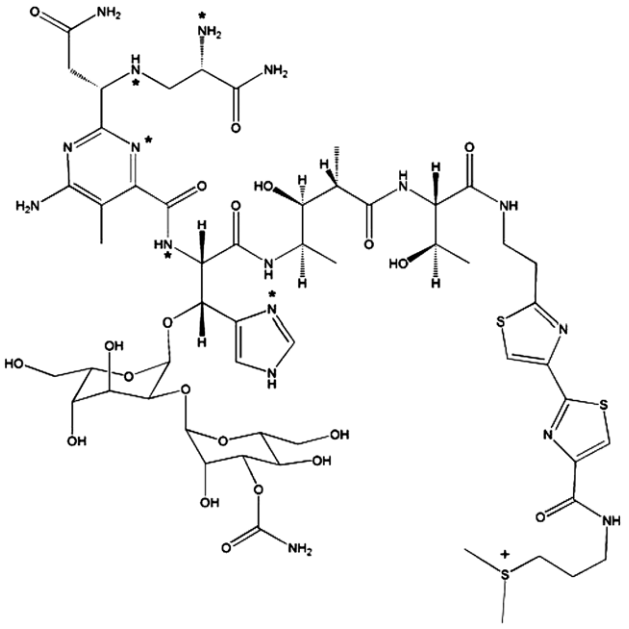

Scheme 1. Chemical structure of bleomycin A_2. The atoms indicated with an asterisk (*) are the ligands for the transition metals Co and Fe.

for selecting the sequence of DNA to be cleaved by BLM, there are evidences that the bithiazole, which is also capable of DNA binding, has its own preferred sequence selectivity. The disaccharide unit is possibly responsible for cell surface recognition and uptake, while it may participate in the metal-binding process [7].

It is generally accepted that the mechanism of the DNA degradation by BLM is both oxygen and metal ion-dependent [5,8–11]. Although BLM is capable of binding several metal ions, i.e., Fe(II), Fe(III) Co(II), Co(III), Ni(II), Ni(III), Cu(II), Zn(II), Cd(II), Ru(II), Rh(III) and Ga(III), the highest activity is observed when is bound to Fe(II) [12–17]. Dioxygen reacts with the Fe(II)BLM in vivo to form the activated BLM, which is a low-spin HOO–Fe(III)BLM complex. There exists some disagreement as to whether HOO–Fe(III)BLM represents the final, active intermediate that directly reacts with DNA or whether a mechanism involving Fe(III)–O–OH bond cleavage leading to a higher ferryl or perferryl species is responsible for initiating DNA strand scission. The activated BLM causes DNA scission via hydrogen abstraction from the C4′of deoxyribose [2].

In order to establish structure–function correlations, determine the basic coordination chemistry of BLM, and give insights into the mechanism of the DNA degradation, much research has been devoted to the elucidation of the structures of some metallo-BLMs (MBLMs). Most of the efforts, however, have been devoted to the determination of the solution structure of MBLMs using spectroscopic methods [i.e., NMR, EPR (electron paramagnetic resonance)] [16–24], theoretical calculations [25–27] or both [28]. In a very recent report, Petering and coworkers [29] presented resonance Raman data that identified two important vibrational modes in the HOO–Co(III)BLM linkage, the stretching modes ν(Co–OOH) and ν(O–OH). Advantage was also taken of the isostructural relationship between Fe(III)BLM and Co(III)BLM to analyze and assign the high-frequency modes for HOO–Co(III)BLM and Co(III)BLM (A_2 and B_2). The obtained data might be useful for future studies of photoactivated CoBLM in an attempt to characterize oxygen-independent DNA damage pathways. It was only until recently, when the crystal structures of a metal free BLM and its Cu(II) complex were determined by X-ray crystallography at resolutions of 1.8 and 1.6 Å, respectively [30]. The crystal structure of the Cu(II)BLM reveals that the Cu(II) centre is penta-coordinate in a square pyramidal environment.

A complementary approach, aiming at providing insights into the structure and function of MBLMs, is the ''synthetic analogue approach'' [31]. In this approach, low molecular weight organic molecules, which resemble or consist of the metal-binding domain of BLM, are utilized as ligands to synthesize metal complexes that serve as models for the MBLMs. These low molecular weight metal complexes are ideally obtainable in crystalline form and can provide structural and spectroscopic data that relate to the MBLM. Pioneer work from Mascharak [32–47] and others [48–55] on the ''synthetic analogue approach'' has provided substantial information about the structure and function of MBLMs described above.

Although FeBLM exhibits the highest activity, many of the synthetic analogues that have been synthesized involve transition metals other than Fe(II) or Fe(III) [32,34–44,48,49,51]. Interestingly, synthetic analogues of BLM with Ga(III) are not known, despite the striking similarities between Fe(III) and Ga(III), i.e., ionic radii, coordination preferences and ionization potentials. This is surprising, considering that early studies by Lenkinski et al. [15] have shown that Ga(III) forms a fairly long lived complex with BLM. More recently, the solution structure of Ga(III)BML (A_2) was elucidated by ^{1}H and ^{13}C NMR [23].

Gallium has been found to accumulate in biological tissues of tumorous nature, thus raising the possibility of its use in radiodiagnostic medicine for the localization, imaging and treatment of aberrant soft tissue [56,57]. Today the biomedical interest of gallium(III) complexes originates from the incorporation of its radionuclides ($^{67}Ga^{3+}$, $^{68}Ga^{3+}$) into diagnostic radiopharmaceuticals [58], the strong antitumour activity of $GaCl_3$ and $Ga(NO_3)_3$ which have been tested in cancer patients [59], and from the moderate in vitro anti-HIV (human immunodeficiency virus) activity of $Ga(NO_3)_3$ and some $GaCl_3$/L complexes (L = various azoles) [60].

Our interest in the bioinorganic chemistry of Ga(III) is primarily focused on the preparation, structural and physical characterization, and evaluation of the biological activity of Ga(III) complexes with biologically relevant ligands [61,62]. In this context, we recently reported the synthesis and characterization of a Ga(III) complex with an orotate-type ligand [62]. Herein we describe the synthesis, single-crystal X-ray structures, IR and ^{1}H NMR characterization of two Ga(III) complexes with a ligand that resembles the metal-binding site of BLM. These products are the first structurally characterized synthetic analogues of BLM with Ga(III).

2. Experimental

2.1. Materials and methods

$(Et_4N)[GaCl_4]$ was prepared as a colourless crystalline powder from the reaction of $Et_4NCl \cdot H_2O$ with $GaCl_3$ (1:1 ratio) in EtOH/H_2O (3:1, v/v). *N*-(2-(4-Imidazolyl)ethyl)pyridine-2-carboxamide (pypepH_2) was prepared by literature methods [32]. All other chemicals and reagents of analytical grade were purchased commercially and used without further purification. C, H and N analyses were conducted by the University of Ioannina, Greece, Microanalytical Service using an EA 1108 Carlo Erba analyzer. Thermogravimetric (TG), differential thermogravimetric (DTG) and differential scanning calorimetry (DSC) data (30–800 °C) were obtained on a TA Instruments SDT 2960 equipment in a dinitrogen gas flow; sample weights of 5-15 mg and a heating rate of 5 °C min^{-1} were used. IR spectra (4000–450 cm^{-1}) were recorded on a Perkin–Elmer 16 PC spectrometer with samples prepared as KBr pellets. ^{1}H NMR spectra in DMSO-d_6 were recorded at 25 °C on an Avance DPX spectrometer of Bruker using a resonance frequency of 400.13 MHz; chemical shifts are quoted on the δ scale and referenced versus external TMS or the protio impurity of the solvent used.

2.2. Syntheses of complexes

2.2.1. $[Ga(pypepH)_2]Cl \cdot 2H_2O$ (**1**)

A solution of pypepH_2 (0.10 g, 0.48 mmol) in EtOH (7 ml) was added to a warm solution (50 °C) of $(Et_4N)[GaCl_4]$ (0.04 g, 0.12 mmol) in the same solvent (7 ml). The colourless solution obtained turned light yellow after stirring for one hour at room temperature. Liquid diffusion of an Et_2O/hexane mixture (30 ml, 1:1 v/v) into the reaction solution produced colourless crystals of **1** over a period of one week. Yield: 0.044 g, 65%. Anal. Calc. for $C_{22}H_{26}N_8O_4GaCl$: C, 46.22; H, 4.58; N, 19.60. Found: C, 46.21; H, 4.51; N, 18.40% IR (KBr pellets, cm^{-1}): 3404 (mb), 3358 (mb), 3292 (w), 3122 (mb), 2916 (wb), 1626 (s), 1594 (s), 1514 (w), 1464 (w), 1390 (s), 1384 (w), 1280 (m), 1188 (m), 1086 (w), 1034 (m), 922 (w), 852 (m), 770 (m), 696 (m), 638 (mb), 530 (w), 500 (w), 456 (w).

2.2.2. $[Ga_4(acac)_4(pypep)_4] \cdot 4.4H_2O$ (**2**)

$Ga(acac)_3$ (0.10 g, 0.28 mmol) and pypepH_2 (0.06 g, 0.28 mmol) were dissolved in 25 ml of Me_2CO to give a colourless solution. Liquid diffusion of Et_2O (50 ml) into the reaction solution yielded colourless crystals of **2** over a period of one week. Yield: 0.045 g, 40%. Anal. Calc. for $C_{64}H_{76.8}O_{16.4}N_{16}Ga_4$: C, 47.70; H, 4.79; N, 13.90. Found: C, 47.62; H, 4.21; N, 13.70%. IR (KBr pellets, cm^{-1}): 3428 (mb), 3074 (w), 2912 (w), 2852 (w), 1632 (s), 1598 (s), 1568 (s), 1526 (s), 1488 (w), 1430 (w), 1384 (s), 1348 (sh), 1290 (m), 1278 (m), 1228 (m), 1194 (w), 1150 (w), 1110 (m), 1058 (m), 1024 (m), 978 (m), 930 (m), 864 (w), 842 (w), 818 (w), 762 (m), 696 (m), 664 (m), 650 (m), 540 (w), 500 (w), 464 (w).

2.3. X-ray crystallographic studies

Data collection, crystal data and structure solution information are given in Table 1. Crystals of **1** and **2** were mounted in air and in capillary, respectively. Diffraction measurements were made on a Crystal Logic dual goniometer diffractometer using graphite-monochromated Mo radiation. Unit cell dimensions were determined and refined using the angular settings of 25 automatically centred reflections in the range $11° < 2\theta < 25°$. Three standard reflections, monitored every 97 reflections, showed less than 3% variation and no decay. Lorentz, polarization and ψ-scan (only for **2**) absorption corrections were applied using Crystal Logic software.

The structures were solved by direct methods using SHELXS-86 [63] and refined by full-matrix least-squares techniques on F^2 with SHELXL-93 [64]. For **1,** all hydrogen atoms were located by difference maps and were refined isotropically; all non-hydrogen atoms were refined anisotropically. For **2,** all hydrogen atoms were located by difference maps and were refined isotropically, except those on the methyl groups with the carbon atoms C(15) and C(16) which were introduced at calculated positions as riding on their respective bonded atoms. All non-hydrogen atoms of the tetranuclear complex were refined anisotropically, except those of the solvate water molecules which were refined isotropically with occupation factors fixed at 10.35, 10.25, 10.20, 10.20 and 10.10 for OW(1), OW(2), OW(3), OW(4) and OW(5), respectively.

The largest shift/esd values in the final cycles were 0.010 (**1**) and 0.001 (**2**).

Table 1
Crystallographic data for complexes $[Ga(pypepH)_2]Cl \cdot 2H_2O$ (**1**) and $[Ga_4(acac)_4(pypep)_4] \cdot 4.4H_2O$ (**2**)

	1	**2**
Empirical formula	$C_{22}H_{26}N_8O_4ClGa$	$C_{64}H_{76.8}N_{16}O_{16.4}Ga_4$
Formula weight	571.68	1611.49
Crystal colour, habit	Colourless, prism	Colourless, prism
Crystal dimensions (mm)	$0.10 \times 0.10 \times 0.50$	$0.20 \times 0.33 \times 0.45$
Crystal system	Triclinic	Tetragonal
Space group	$P\bar{1}$	$I4_1/a$
a (Å)	9.473(4)	22.71(1)
b (Å)	10.946(5)	22.71(1)
c (Å)	13.212(5)	16.32(7)
α (°)	92.678(15)	90
β (°)	108.45(1)	90
γ (°)	105.59(1)	90
V (Å^3)	1238.6(9)	8418(6)
Z	2	4
D_{calc} (g/cm^{-3})	1.533	1.272
F(0 0 0)	588	3312
μ (mm^{-1})	1.265	1.332
Radiation (λ, Å)	0.71073	0.71073
Temperature (K)	298	298
Scan mode	θ–2θ	θ–2θ
Scan speed (° min^{-1})	3.0	1.5
Scan range (°)	2.2 + α_1 α_2 separation	2.2 + α_1 α_2 separation
θ Range (°)	1.95–25.03	2.36–25.00
h k l ranges	−10–11; −13–13; −15–0	−27–0; 0–27; 0–19
Reflections collected	4564	3983
Independent reflections(R_{int})	4356 (0.0157)	3643 (0.0481)
Number of refined parameters	429	283
Observed reflections [$I > 2\sigma(I)$]	4020	2402
GOF (on F^2)	1.047	1.119
Final R indices[a] [$I > 2\sigma(I)$]	$R_1 = 0.0296$, $wR_2 = 0.0776$	$R_1 = 0.0493$, $wR_2 = 0.1124$
R indices[a] (all data)	$R_1 = 0.0328$, $wR_2 = 0.0806$	$R_1 = 0.0996$, $wR_2 = 0.1330$
Largest difference peak and hole (e Å^{-3})	0.550 and −0.363	0.394 and −0.324

[a] Defined as: $R_1 = \sum(|F_o| - |F_c|)/\sum(|F_o|), wR_2 = \{\sum[w(F_o^2 - F_c^2)/\sum[w(F_o^2)^2]\}^{1/2}$, where $w = 1/[\sigma^2(F_o^2) + (aP)^2 + (bP)]$ with $P = [\max(F_o^2, 0) + 2F_c^2]/3$.

3. Results and discussion

3.1. General information

The ligand *N*-(2-(4-imidazolyl)ethyl)pyridine-2-carboxamide ($pypepH_2$, Scheme 2, Hs refer to the two potentially dissociable amide and imidazolyl hydrogens) contains three nitrogen donor centres located on the pyridine and imidazole rings, and the amide moiety, and thus (with the assumption that the pyridyl nitrogen models the donor nitrogen atom of the pyrimidine ring in the native system) resembles part of the metal-chelating region of BLM, see Scheme 1. It was first designed and synthesized by Mascharak's group in an attempt to create metal complexes that match the metal coordination environment in MBLMs. This group isolated and structurally characterized two dinuclear Cu(II) complexes, namely $[Cu_2(O_2CMe)_2(pypepH)_2] \cdot 1.46H_2O$ (**3**) [32] and $[Cu_2Cl_2(pypepH)_2] \cdot 2H_2O$ (**4**) [35], and two mononuclear complexes with Co(III) and Fe(III), namely $[Co(pypepH)_2]ClO_4 \cdot H_2O$ (**5**) [34] and $[Fe(pypepH)_2]Cl \cdot 2H_2O$ (**6**) [33].

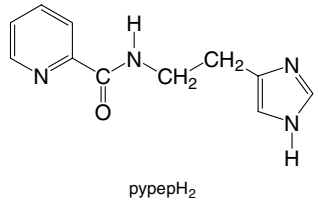

$pypepH_2$

Scheme 2. The neutral ligand *N*-(2-(4-imidazolyl)ethyl)pyridine-2-carboxamide ($pypepH_2$) used in this work.

In all four complexes, the monoanion of $pypepH_2$, $pypepH^-$, adopts the coordination mode shown in Scheme 3 and chelates to a metal ion through the pyridyl, the deprotonated amide and the imidazolyl nitrogen atoms. In the dinuclear complexes **3** and **4,** the Cu^{II} centres adopt a distorted square pyramidal geometry, each being chelated by one $pypepH^-$ ligand and doubly bridged to the second Cu^{II} centre by monoatomic $MeCO_2^-$ and Cl^- anions, respectively. In **5** and **6**, the metal centres are in an octahedral environment created by two tridentate chelating $pypepH^-$ ligands in a *mer* configuration.

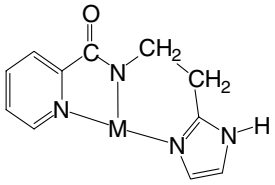

Scheme 3. The crystallographically established coordination mode of the monoanionic ligand pypepH$^-$.

3.2. Synthetic aspects

$[Ga(pypepH)_2]Cl \cdot 2H_2O$ (**1**) was first isolated from the reaction of $(Et_4N)[GaCl_4]$ with four equivalents of $pypepH_2$ in EtOH. A similar reaction involving $(Et_4N)[FeCl_4]$ and the same ligand yielded [33] the mononuclear complex **6**. The $pypepH_2$:Ga^{III} reaction ratio has no influence on the identity of product; complex **1** can be isolated using either a 2:1 or an 1:1 ratio. Its stoichiometric preparation is summarized in Eq. (1). The ability of the ligand to undergo gallium(III)-promoted

$$(Et_4N)[GaCl_4] + 2pypepH_2 + 2H_2O \xrightarrow{EtOH} [Ga(pypepH_2)]Cl \cdot 2H_2O + Et_4NCl + 2HCl \quad (1)$$

deprotonation at acidic "pH" is of remarkable chemical interest [65]. The solvate water molecules in crystalline **1** derived from either the solvent or the atmosphere during the crystallization step.

The preparation of the tetranuclear complex $[Ga_4(acac)_4(pypep)_4] \cdot 4.4H_2O$ (**2**) is summarized in Eq. (2):

$$4Ga(acac)_3 + 4pypepH_2 + 4.4H_2O \xrightarrow{Me_2CO} [Ga_4(acac)_4(pypep)_4] \cdot 4.4H_2O + 8acacH \quad (2)$$

Treatment of $Ga(acac)_3$ with $pypepH_2$ in a 1:1 molar ratio in Me_2CO led to a colourless solution, from which colourless crystals of **2** were isolated after liquid diffusion with Et_2O. The tetranuclear complex **2** has doubly deprotonated ions of $pypepH_2$ as ligands; this is a consequence of the high acac$^-$ to $pypepH_2$ ratio (3:1) used in the reaction. Thus, the acetylacetonate ion plays a double role in the reaction. It is necessary for the double deprotonation of $pypepH_2$ acting as a strong base and participates in the product as a ligand. Treatment of tris(acetylacetonato)gallium(III) with two or three equivalents of $pypepH_2$ leads to the same product in various yields. Despite our efforts, no gallium(III), acac$^-$-free complex containing the dianion of the ligand, e.g., $Ga_2(pypep)_3$, could be prepared.

3.3. Description of structures

An ORTEP diagram of the cation of **1** is shown in Fig. 1. Selected bond distances, angles and hydrogen bonding details are given in Table 2. Complex **1** is isostructural to **6** [33]. Its structure consists of the mononuclear cation $[Ga(pypepH)_2]^+$, one Cl$^-$ counterion and two H_2O solvate molecules. The Ga^{III} atom is in a distorted octahedral environment, with the *cis* angles of the octahedron in the 78.75–97.40° range and the *trans* angles in the narrow 168.76–169.47° range. Two tridentate chelating pypepH$^-$ anions are coordinated to the metal ion through the pyridyl, the deprotonated amide(peptide) and the pyridine-type imidazolyl nitrogen atoms. The pyridyl and imidazolyl donor atoms of the same anion are *trans* to each other. The two pypepH$^-$ chelate the Ga^{III} centre having their deprotonated amide nitrogens *trans* to each other, thus leading to the *mer* isomer. The Ga–N bond distances are in the 2.007(2)–2.033(2) Å range for the imidazolyl and peptide nitrogen atoms, and are slightly shorter than those involving the pyridyl nitrogen atoms [Ga–N = 2.141(2) and 2.152(2) Å]. The N–Ga–N angles that show maximum deviation from octahedral values are the angles N(1)–Ga–N(2) [78.82(7)°] and N(21)–Ga–N(22) [78.75(8)°] involving the pyridyl and deprotonated amide(peptide) nitrogens. This might arise [33] from the presence of a short (bond order >1) amide C–N bond in the five-membered chelating rings.

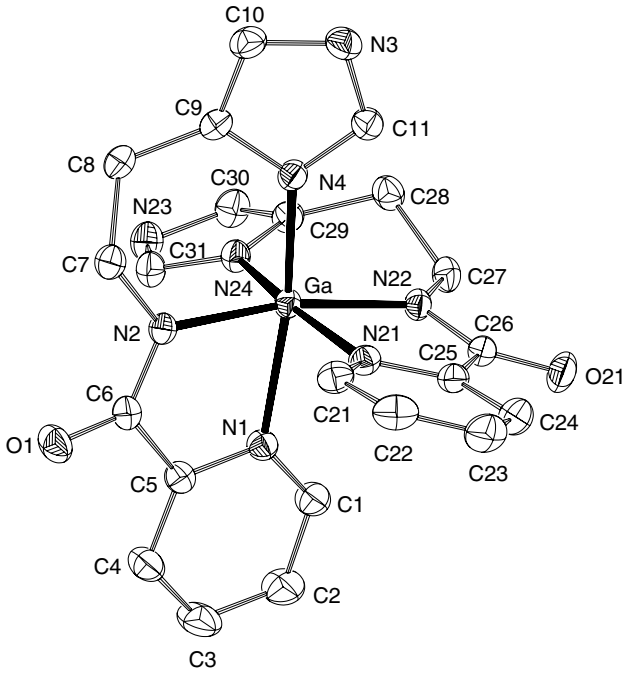

Fig. 1. A labeled ORTEP plot of $[Ga(pypepH)_2]^+$, showing 30 % probability ellipsoids. Hydrogen atoms have been omitted for clarity.

The Ga–N(pyridyl) bond lengths are close to those in other structurally characterized complexes containing Ga^{III}–*N*-(2-pyridyl) bonds [66]. The geometries of the pyridine and imidazole rings are regular [33].

The two crystallographically unique water molecules act as both hydrogen bond donors and acceptors to the peptide oxygen atoms and the imidazolyl NH moieties,

Table 2
Selected interatomic distances (Å), angles (°) and hydrogen bond dimensions for complex $[Ga(pypepH)_2]Cl \cdot 2H_2O$ (**1**)

Ga–N(22)	2.007(2)	N(4)–Ga–N(24)	94.11(8)
Ga–N(2)	2.011(2)	N(22)–Ga–N(21)	78.75(8)
Ga–N(4)	2.024(2)	N(2)–Ga–N(21)	93.82(8)
Ga–N(24)	2.033(2)	N(4)–Ga–N(21)	90.24(7)
Ga–N(21)	2.141(2)	N(24)–Ga–N(21)	169.47(7)
Ga–N(1)	2.152(2)	N(22)–Ga–N(1)	92.34(7)
N(22)–Ga–N(2)	168.76(7)	N(2)–Ga–N(1)	78.82(7)
N(22)–Ga–N(4)	97.40(7)	N(4)–Ga–N(1)	169.40(7)
N(2)–Ga–N(4)	90.99(7)	N(24)–Ga–N(1)	89.85(7)
N(22)–Ga–N(24)	91.17(8)	N(21)–Ga–N(1)	87.56(7)
N(2)–Ga–N(24)	95.69(8)		
D–H···A	D···A	H···A	∠DHA
N(3)-H(N3)···O(W2)	2.748(1)	2.000(1)	148.24(4)
N(23)-H(N23)···O(W1)	2.751(1)	2.058(1)	153.66(3)
O(W1)-H(W1B)···O(1)^{i}	2.794(1)	2.088(1)	163.70(4)
O(W2)-H(W2B)···O(21)^{ii}	2.824(1)	2.070(1)	165.90(4)
O(W1)-H(W1A)···Cl^{iii}	3.138(1)	2.396(1)	168.08(4)
O(W2)-H(W2A)···Cl	3.133(1)	2.325(1)	169.22(4)

Symmetry transformations: (i) $-x+1, -y, -z$; (ii) $-x+1, -y+1, -z+1$; (iii) $-x+1, -y+1, -z$.
A, acceptor and D, donor.

respectively. As a result of the hydrogen bonding pattern, one-dimensional chains involving the $[Ga(pypepH)_2]^+$ cations and the water molecules form in the crystal lattice (Fig. 2).

The hydrogen bonded chains are further bridged via H–O–H···Cl^- hydrogen bonds to form an overall two-dimensional hydrogen bonded layer as shown in Fig. 3.

The cation of complex **1** has a remarkably similar structure with the cations present in complexes **5** and **6** [33,34].

A labeled ORTEP plot of the coordination environment around the Ga^{III} atom in complex **2** is shown in Fig. 4. Selected bond distances and angles are listed in Table 3.

The components in **2** assemble to form a discrete tetranuclear complex (Fig. 5). Complex **2** crystallizes in the tetragonal space groups $I4_1/a$. There is a fourfold inverse crystallographic axis, i.e., $\overline{4}$, in the centre of the cyclic tetramer. Each Ga^{III} atom is then crystallographically equivalent within the tetramer. The dianion of the $pypepH_2$ ligand, $pypep^{2-}$, chelates one Ga^{III} atom through the pyridyl, the deprotonated amide and one of the imidazolate nitrogen atoms, and bridges a second Ga^{III} atom through the other imidazolate nitrogen (Scheme 4). The Ga^{III} atom, which adopts a slightly distorted octahedral geometry, is coordinated to three nitrogen atoms of a tridentate chelating $pypep^{2-}$ ligand and to the imidazolate nitrogen atom of a second neighbouring ligand. The pyridyl and imidazolate N atoms of the same anion are *trans* to each other, while the imidazolate N atom of the second ligand is in a *cis* configuration to all donor atoms of the first chelating ligand. One bidentate chelating $acac^-$ ligand completes the coordination sphere at the metal centre. Thus, the donor set for each Ga^{III} atom consists of four nitrogen atoms from $pypep^{2-}$ and two oxygen atoms from $acac^-$. Three Ga–N distances are in the 1.990(4)–2.047(4) Å range, with the pyridyl nitrogen forming a slightly longer bond with the Ga^{III} atom [Ga–N(4) = 2.118(4) Å]. The latter

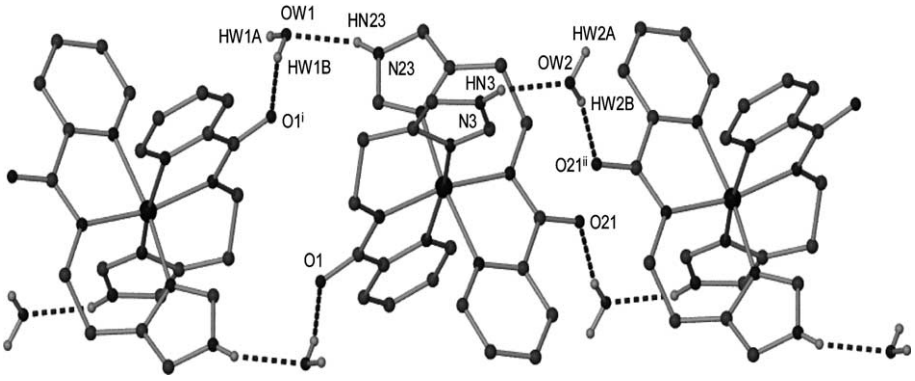

Fig. 2. The hydrogen-bonded chain formed by the cation $[Ga(pypepH)_2]^+$ and the lattice water molecules in the crystal of **1**.

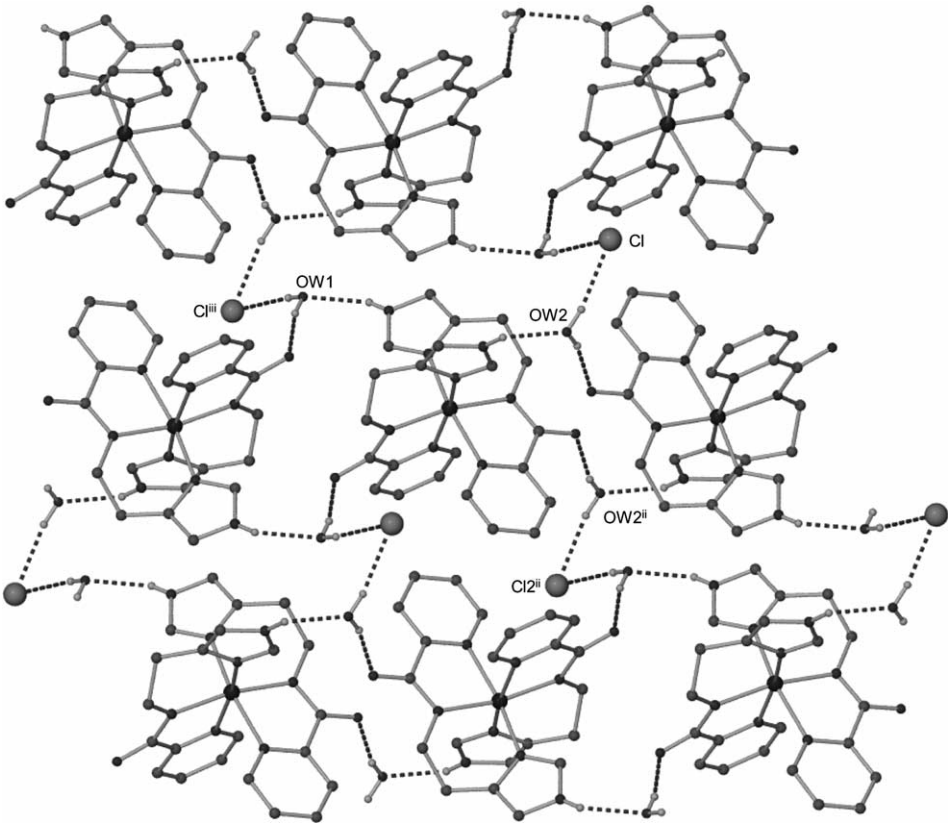

Fig. 3. The overall two-dimensional hydrogen bonded layer in the crystal structure of **1**.

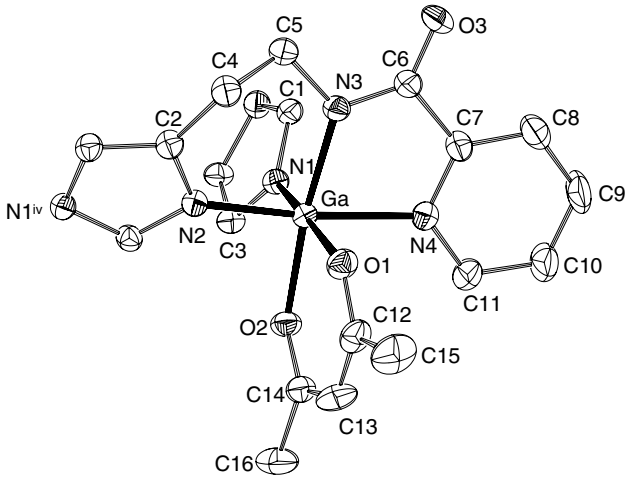

Fig. 4. A labeled ORTEP plot of the coordination environment of the Ga^{III} atom in complex **2** showing 30 % probability ellipsoids. The symmetry operation for N(1) is: (iv) $x - 0.25$, $-y + 0.75$, $-z + 0.75$. Hydrogen atoms have been omitted for clarity.

distance is slightly longer than the Ga–N(pyridyl) bond lengths observed in **1** [average 2.146(2) Å]. The Ga–N(deprotonated amide) bond length [1.990(4) Å] compares well with the respective distances observed [average 2.009(2) Å] in the mononuclear cation of **1**. There are two types of Ga(III)–N(imidazolate) bonds

Table 3
Selected interatomic distances (Å) and angles (°) for complex $[Ga_4(acac)_4(pypep)_4] \cdot 4.4H_2O$ (**2**)

Ga–O(2)	1.979(3)	N(2)–Ga–N(1)	93.2(2)
Ga–N(3)	1.990(4)	O(2)–Ga–O(1)	87.6(2)
Ga–N(2)	1.995(4)	N(3)–Ga–O(1)	91.2(2)
Ga–N(1)	2.047(4)	N(2)–Ga–O(1)	92.6(2)
Ga–O(1)	2.046(4)	N(1)–Ga–O(1)	171.0(2)
Ga–N(4)	2.118(4)	O(2)–Ga–N(4)	93.8(2)
O(2)–Ga–N(3)	173.5(2)	N(3)–Ga–N(4)	79.8(2)
O(2)–Ga–N(2)	93.2(2)	N(2)–Ga–N(4)	172.7(2)
N(3)–Ga–N(2)	93.3(2)	N(1)–Ga–N(4)	89.5(2)
O(2)–Ga–N(1)	85.2(2)	O(1)–Ga–N(4)	85.5(2)
N(3)–Ga–N(1)	95.3(2)		

in **2**. The Ga–N bond length [Ga–N(2) = 1.995(4) Å] for the first type, which consists of a bond within the "Ga(pypep)" unit, is shorter than the Ga–N bond length [Ga–N(1) = 2.047(4) Å] for the second type that connects "Ga(pypep)" units; the observed difference is a consequence of the chelate effect. The Ga–N(2) bond length in **2** is slightly shorter than the corresponding distances [average 2.029(2) Å] in **1**. This may be due to the fact that in **1** the ligand framework contains an *imidazole* moiety as compared to the *imidazolate* group present in **2**. The Ga–O distances of 1.979(3) and 2.046(4) Å are in the range observed in other octahedral Ga(III) complexes involving acetylacetonate donor groups [67].

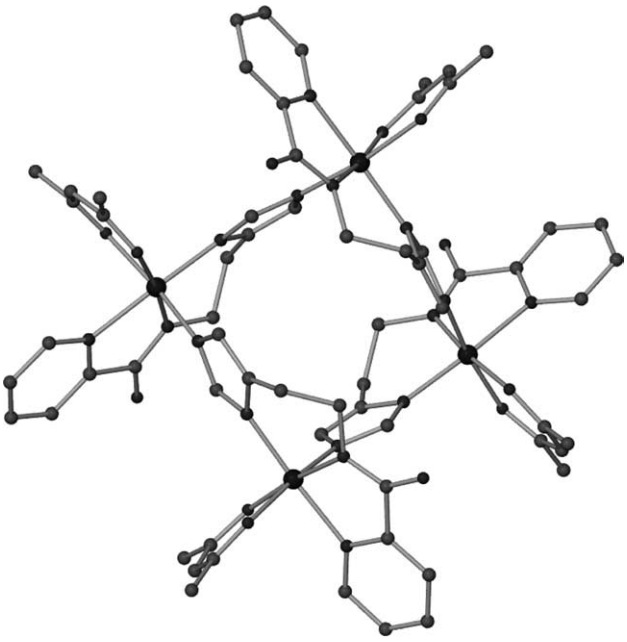

Fig. 5. Ball and stick representation of the tetranuclear assembly $[Ga_4(acac)_4(pypep)_4]$ of complex **2**.

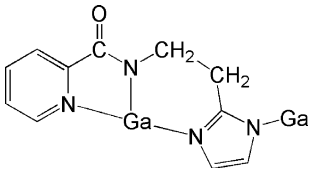

Scheme 4. The crystallographically established coordination mode of the dianionic ligand $pypep^{2-}$ in complex **2**.

The shape of the tetranuclear complex as shown in Fig. 5 reminisces of a square, with sides of 6.030 Å and diagonals of 8.008 Å (Ga···Ga distances). However, a closer look of the structural data reveals that the four Ga^{III} atoms are not arranged at the corners of a perfect square. The average deviation of each Ga^{III} atom from the mean plane formed by the four metal ions is 0.26 Å, while the Ga···Ga···Ga angle, and the torsion angle between the four Ga^{III} atoms are 83.21° and 38°, respectively.

This topology is better described as "butterfly" [68] rather than square (Fig. 6).

Fig. 5 illustrates the presence of an empty space in the central region of the molecule of **2**. However, the space filling model of the compound (Fig. 7) clearly shows that there is no room left for a potential guest molecule. There are five disordered water molecules per asymmetric unit in the crystal with occupancies of 10%, 20%, 20%, 25% and 35%.

3.4. ^1H NMR spectrum of complex 1

The ^1H NMR spectrum of the mononuclear complex in DMSO-d_6 is shown in Fig. 8. The assignment of the

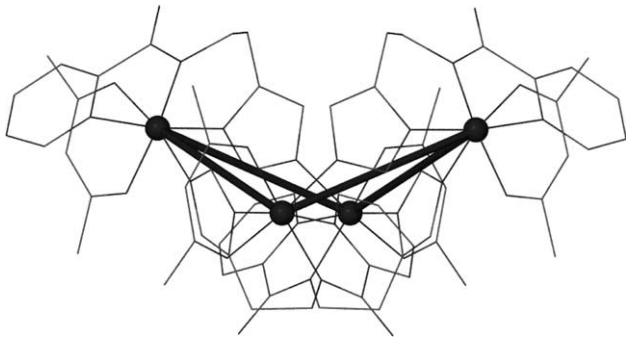

Fig. 6. A view of the tetranuclear assembly $[Ga_4(acac)_4(pypep)_4]$ of complex **2** showing the "butterfly" like topology of the metal ions. The thick lines connecting the Ga^{III} atoms are guides for the eye.

resonances has been achieved by the comparison of this spectrum with the spectra of complex $[Co(pypepH)_2]$-$ClO_4 \cdot H_2O$ (**5**) [34] and the free ligand [35]. As in the case of **5**, the ^1H NMR spectrum of **1** suggests that the integrity of the cation $[Ga(pypepH)_2]^+$ is maintained in the DMSO solution. Specifically, in the ^1H NMR of the free ligand, the two CH_2 groups appear as a triplet at 2.88 and a quartet at 3.66 ppm, respectively. In the case of **1**, these four H atoms resonate at four different positions, forming a doublet, triplet, doublet, triplet (dtdt) pattern in the 5–2.5 ppm region. The dtdt pattern of these H atoms suggests that the $pypepH^-$ anions are held in space quite rigidly in the chelate ring around the Ga(III) centre [34,38]. The protons of the H_2O molecules resonate at 3.33 ppm; the peak disappears on addition of D_2O. The imidazole NH peak shifts from 9.0

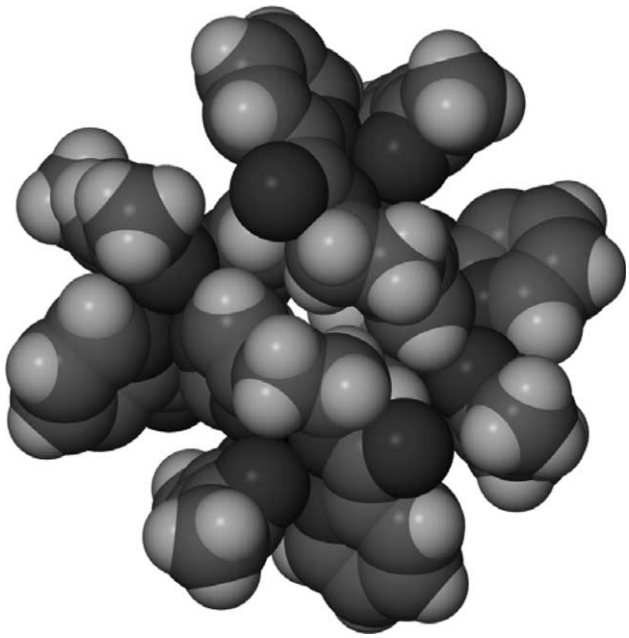

Fig. 7. Space filling model of the tetranuclear complex $[Ga_4(acac)_4(pypep)_4]$.

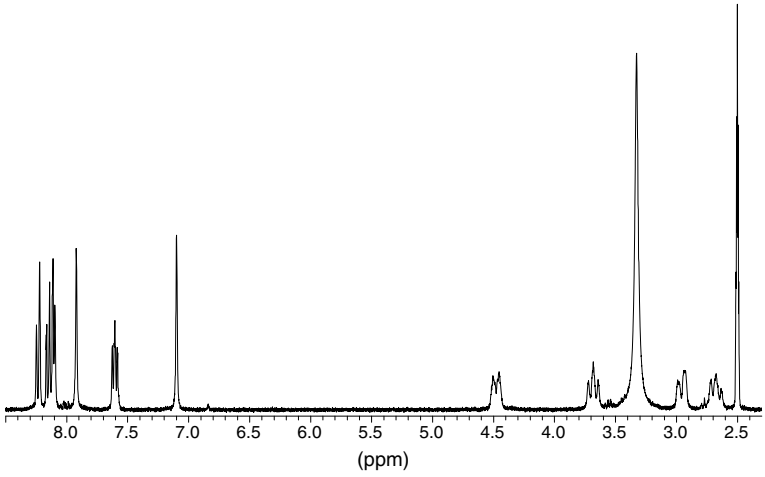

Fig. 8. The ^{1}H NMR spectrum of **1** in DMSO-d_6 at room temperature. The signal at 3.33 ppm is due to the lattice H_2O molecules and that at 2.50 ppm is due to residual protons in the solvent. The imidazole NH signal (present at ~12.6 ppm) is not shown.

ppm in free pypepH$_2$ to ~12.6 ppm in the complex, presumably because the donation of electron density by the pyridine-type imidazole nitrogens to gallium(III) results in deshielding of the protons bound to the other imidazole nitrogen [34]. The NH signal is broad and disappears on addition of D_2O. Although the pattern of the ^{1}H NMR spectrum of **1** is the same with that of **5**, the resonances of all peaks are slightly shifted both upfield and downfield, due to the different electronic configurations of Co(III) and Ga(III). Due to the poor solubility of **2** in all organic solvents and H_2O, we were unable to record its NMR spectrum.

3.5. IR spectra and thermal decomposition data

In the ν(OH) region, the IR spectra of the complexes exhibit medium-intensity bands at 3404, 3358 (**1**) and 3428 (**2**) cm^{-1}, assignable to $\nu(OH)_{\text{lattice water}}$ [69]. The broadness and the relatively low frequency of these bands are both indicative of hydrogen bonding. The medium, broadband at 3122 cm^{-1} in the spectrum of **1** is assigned [32] to the $\nu(NH)_{\text{imidazole}}$ mode; this band appears at 3110 cm^{-1} in free pypepH$_2$. As would be expected from the stoichiometry, the $\nu(NH)_{\text{imidazole}}$ band is absent in the spectrum of **2.**

The amide II and III bands [due to δ $(NH)_{\text{amide}}$ + $\nu(C–N)_{\text{amide}}$ in compounds containing neutral *trans* secondary amide groups] have been replaced by a new strong absorption at 1390 (**1**) and 1384 (**2**) cm^{-1}, which is characteristic for deprotonated secondary (in fact tertiary) amide complexes [70]; this replacement might be expected, since on removal of the amide proton the band becomes a pure C–N stretch. The $\nu(C{=}O)_{\text{amide}}$ [amide I] band (observed at 1678 cm^{-1} in free ligand) appears at 1626 and 1632 cm^{-1} in the spectra of **1** and **2**, respectively; this large low-frequency shift is typical of deprotonated amide N-bonding [70].

The characteristic in-plane and out-of-plane deformation bands of the 2-pyridyl ring of free pypepH$_2$ at 630 and 421 cm^{-1}, respectively, are shifted upwards in **1** (638 and 456 cm^{-1}) and **2** (650 and 464 cm^{-1}), indicating the involvement of the ring N-atom in bonding to gallium(III) [71].

The ν(C=C), ν(C=O), δ(CH), $\delta_d(CH_3)$ modes of the acetylacetonate ligand are expected to appear [72] at 1616–1395 cm^{-1} in the spectrum of **2**; however, contributions from a plethora of vibrations [ν(C=N), ν(C=N), ν(C=C), ν(C=C), $\delta(CH_2)$], also expected in this region, renders assignments difficult.

Complex **1** decomposes via an anhydrous stable intermediate. The thermal data show an initial, endothermic weight loss between 68 and 125 °C, which corresponds exactly to the release of all the water content (found: 6.31; calc.: 6.30%). A clear plateau is reached at about 130 up to 160 °C, suggesting that the anhydrous species is thermally stable. The formation of the anhydrous compound is illustrated in Eq. (3). The anhydrous product, obtained after a TG experiment up to 144 °C by keeping the heating rate at 1 °C min^{-1}, was isolated (temperature-arrest technique); its IR spectrum is also identical with that of **1**, but it does not exhibit the water bands. The anhydrous intermediate decomposes above 160 °C with a rather simple degradation mechanism, as revealed by the appearance of two broad DTG maxima at 292 and 455 °C, and without the formation of a new stable intermediate. Decomposition above 500 °C is slow and continues at 800 °C.

$$\underset{\mathbf{1}}{[\mathrm{Ga(pypepH)_2}]\,\mathrm{Cl}\cdot 2\mathrm{H_2O}} \overset{68-125^{\circ}\mathrm{C}}{\underset{\mathrm{N_2}}{\rightarrow}} [\mathrm{Ga(pypepH)_2}]\mathrm{Cl} + 2\mathrm{H_2O}\uparrow \quad (3)$$

Complex **2** releases all the water content in two endothermic steps between 55 and 120 °C. The absence of TG plateaux between 55 and 120 °C indicates

that stable hydrated intermediates cannot be formed. Clear plateaux are not reached after complete dehydration, because a multistep (as indicated by the large number of inflections in the TG curve and of maxima in the DTG curve) decomposition of the anhydrous species starts immediately. The final decomposition product does not correspond to any stoichiometric compound.

4. Summary and concluding comments

The following points are the principal results and conclusions of this investigation.

(1) We have synthesized and structurally characterized a mononuclear gallium(III) complex and a tetranuclear gallium(III) cluster of a ligand resembling a portion of metal-chelating domain of BLM. This is the first synthetic analogue approach to MBLMs using gallium(III).
(2) The tetranuclear cluster **2** is the first structurally characterized complex of any metal containing the dianionic form of pypepH_2, i.e., pypep^{2-}. This form bridges two metal ions.
(3) It is believed that in general Ga(III) has no propensity of promoting amide deprotonation with concominant coordination of the negative amido nitrogen donor centres [65]. The isolation and characterization of **1** and **2** does not support this view. The ability of pypepH_2 to coordinate to Ga(III) via amide deprotonation can be ascribed in part to the presence of additional coordinating donor groups that serve to prevent hydrolysis and precipitation of gallium(III) hydroxide.
(4) The mononuclear complex **1** is isostructural to [Fe(pypep)$_2$]Cl · 2H_2O [33], emphasizing further the view that gallium(III) is the diamagnetic mimic of iron(III) [67], and
(5) The molecular structure of **1** is in agreement with and supports the solution structure of the 1:1 Ga^{III}–bleomycin A_2 complex that has been determined [23] using 2D NMR methods in combination with molecular dynamics calculations. The favoured model in solution is a five-coordinate complex with the primary amine of β-aminoalanine holding the axial position of a distorted square pyramid, and with the secondary amine of *β*-aminoalanine, one pyrimidine nitrogen, the deprotonated histidine amide and the pyridine-type imidazole nitrogen defining the basal plane; no evidences for the disaccharide moiety or the carbamoyl amide coordination were found. Three of the proposed donor atom in the solution structure are also coordinated to gallium(III) in the synthetic analogue **1**.

5. Supplementary material

Crystallographic data (excluding structure factors) in CIF format for the structural analysis have been deposited with the Cambridge Crystallographic Data Centre, CCDC Nos 240412 (**1**) and 240413 (**2**). Copies of this information may be obtained free of charge from the Director, CCDC, 12 Union Road, Cambridge CB2 1EZ, UK (Fax: +44-1223-336033; e-mail: deposit@ccdc.cam.ac.uk or http://www.ccdc.cam.ac.uk).

References

[1] Y. Sugiura, T. Takita, H. Umezawa, in: H. Sigel (Ed.), Metal Ions in Biological Systems, vol. 19, Marcel Dekker, New York, 1985, p. 81.
[2] D.L. Boger, H. Cai, Angew. Chem. Int. Ed. 38 (1999) 448.
[3] S.M. Hecht, Acc. Chem. Res. 19 (1986) 383.
[4] J. Stubbe, J.W. Kozarich, W. Wu, D.E. Vanderwall, Acc. Chem. Res. 98 (1998) 1153.
[5] J. Stubbe, J.W. Kozarich, Chem. Rev. 87 (1987) 1107.
[6] A.T. Abraham, J.-J. Lin, D.L. Newton, S. Rybak, S.M. Hecht, Chem. Biol. 10 (2003) 45.
[7] C.J. Thomas, M.M. McCormick, C. Vialas, Z.-F. Tao, C.J. Leitheiser, M.J. Rishel, X. Wu, S.M. Hecht, J. Am. Chem. Soc. 124 (2002) 3875.
[8] Y. Suguria, T. Suzuka, M. Otsuka, S. Kobayashi, T. Ohno, T. Takita, H. Umezawa, J. Biol. Chem. 258 (1983) 1328.
[9] S.J. Sucheck, J.F. Ellena, S.M. Hecht, J. Am. Chem. Soc. 129 (1998) 7450.
[10] R.M. Burger, Chem. Rev. 98 (1998) 1153.
[11] C.A. Claussen, E.C. Long, Chem. Rev. 99 (1999) 2797.
[12] J.C. Dabrowiak, J. Inorg. Biochem. 13 (1980) 317.
[13] R.C. Brooks, P. Canorhan, J.F. Vallano, N.A. Powell, J.F. Sorakowski, S. Martelluci, M.C. Darkes, S.P. Fricker, B.A. Murrier, Nucl. Med. Biol. 26 (1999) 421.
[14] M.S. Ward, F.-T. Lin, R.E. Shepherd, Inorg. Chim. Acta 343 (2003) 231.
[15] R.E. Lenkinski, B.E. Peerce, J.L. Dallas, J.D. Glickson, J. Am. Chem. Soc. 102 (1980) 131.
[16] C. Vanbelle, B. Brutscher, M. Blackledge, C. Muhle-Goll, M.-H. Remy, J.-M. Masson, D. Marion, Biochemistry 42 (2003) 651.
[17] C. Xia, F.H. Forsterling, D.H. Petering, Biochemistry 42 (2003) 6559.
[18] S.T. Hoehn, H.D. Junker, R.C. Bunt, C.J. Turner, J. Stubbe, Biochemistry 40 (2001) 5894.
[19] K.E. Loeb, J.M. Zaleski, C.D. Hess, S.M. Hecht, E.I. Solomon, J. Am. Chem. Soc. 120 (1998) 1249.
[20] B. Mouzopoulou, H. Kozlowski, N. Katsaros, A. Garnier-Suillerot, Inorg. Chem. 40 (2001) 6923.
[21] C. Zhao, C. Xia, Q. Mao, H. Forsterling, E. DeRose, W.E. Antholine, W.K. Subczynski, D.H. Petering, J. Inorg. Biochem. 91 (2002) 259.
[22] E.C. Wasinger, K.L. Zaleski, B. Hedman, K.O. Hodgson, E.I. Solomon, J. Biol. Inorg. Chem. 7 (2002) 157.
[23] A. Papakyriakou, B. Mouzopoulou, N. Katsaros, J. Biol. Inorg. Chem. 8 (2003) 549.
[24] J.N. Kemsley, K.L. Zaleski, M.S. Chow, A. Decker, E.Y. Shishova, E.C. Wasinger, B. Hedman, K.O. Hodgson, E.I. Solomon, J. Am. Chem. Soc. 125 (2003) 10810.
[25] F. Fedeles, M. Zimmer, Inorg. Chem. 40 (2001) 1557.
[26] M. Freindorf, P.M. Kozlowski, J. Phys. Chem. A 105 (2001) 7267.
[27] T.E. Lehmann, J. Biol. Inorg. Chem. 7 (2002) 305.

[28] F. Neese, J.M. Zaleski, K.L. Zaleski, E.I. Solomon, J. Am. Chem. Soc. 122 (2000) 11703.
[29] C. Rajani, J.R. Kincaid, D.H. Petering, J. Am. Chem. Soc. 126 (2004) 3829.
[30] M. Sugiyama, T. Kumagai, M. Hayashida, M. Maruyama, Y. Matoba, J. Biol. Chem. 277 (2002) 2311.
[31] J.A. Ibers, R.H. Holm, Science 209 (1980) 223.
[32] S.J. Brown, X. Tao, D.W. Stephan, P.K. Mascharak, Inorg. Chem. 25 (1986) 3377.
[33] X. Tao, D.W. Stephan, P.K. Mascharak, Inorg. Chem. 26 (1987) 754.
[34] K. Delany, S.K. Arora, P.K. Mascharak, Inorg. Chem. 27 (1988) 705.
[35] S.J. Brown, X. Tao, T.A. Wark, D.W. Stephan, P.K. Mascharak, Inorg. Chem. 27 (1987) 1581.
[36] S.J. Brown, P.K. Mascharak, D.W. Stephan, J. Am. Chem. Soc. 110 (1988) 1996.
[37] S.J. Brown, S.E. Hudson, D.W. Stephan, P.K. Mascharak, Inorg. Chem. 28 (1989) 468.
[38] M. Muetterties, P.K. Mascharak, Inorg. Chim. Acta 160 (1989) 123.
[39] S.J. Brown, S.E. Hudson, P.K. Mascharak, J. Am. Chem. Soc. 111 (1989) 6446.
[40] S.J. Brown, M.M. Olmstead, P.K. Mascharak, Inorg. Chem. 28 (1989) 3720.
[41] L.A. Scheich, P. Gosling, S.J. Brown, M.M. Olmstead, P.K. Mascharak, Inorg. Chem. 30 (1991) 1677.
[42] J.D. Tan, S.E. Hudson, S.J. Brown, M.M. Olmstead, P.K. Mascharak, J. Am. Chem. Soc. 114 (1992) 3841.
[43] E. Farinas, J.D. Tan, N. Baidya, P.K. Mascharak, J. Am. Chem. Soc. 115 (1993) 2996.
[44] R.H. Guarjado, S.G. Hudson, S.J. Brown, P.K. Mascharak, J. Am. Chem. Soc. 115 (1993) 7971.
[45] E. Farinas, N. Baidya, P.K. Mascharak, Inorg. Chem. 33 (1994) 5970.
[46] K.E. Loeb, J.M. Zaleski, T.E. Westre, R.J. Guarjado, P.K. Mascharak, B. Hedman, K.O. Hodgson, E.I. Solomon, J. Am. Chem. Soc. 117 (1995) 4545.
[47] C. Nguyen, R.J. Guajardo, P.K. Mascharak, Inorg. Chem. 35 (1996) 6273.
[48] E. Kimura, H. Kurosaki, Y. Kurogi, M. Shionoya, M. Shiro, Inorg. Chem. 31 (1992) 4314.
[49] H. Kurosaki, K. Hayashi, Y. Ishikawa, M. Goto, K. Inada, I. Taniguchi, M. Shionoya, E. Kimura, Inorg. Chem. 38 (1999) 2824.
[50] H. Kurosaki, Y. Ishikawa, K. Hayashi, M. Sumi, Y. Tanaka, M. Goto, K. Inada, I. Taniguchi, M. Shionoya, H. Matsuo, M. Sugiyama, E. Kimura, Inorg. Chim. Acta 294 (1999) 56.
[51] H. Kurosaki, K. Hayashi, M. Goto, M. Shionoya, E. Kimura, Inorg. Chem. Commun. 3 (2000) 107.
[52] M. Otsuka, M. Yoshida, S. Kobayaski, M. Ohno, Y. Sugiura, T. Takita, H. Umezawa, J. Am. Chem. Soc. 103 (1981) 6986.
[53] Y. Sugano, A. Kittaka, M. Otsuka, M. Ohno, Y. Sugiura, H. Umezawa, Tetrahedron Lett. 27 (1986) 3635.
[54] T.J. Lomis, J.F. Siuda, R.E. Shepherd, J. Chem. Soc., Chem. Commun. (1988) 290.
[55] J. Kohda, K. Shinozuka, H. Sawai, Tetrahedron Lett. 36 (1995) 5575.
[56] M. Matzapetakis, M. Kourgiantakis, M. Dakanali, C.P. Raptopoulou, A. Terzis, A. Lakatos, T. Kiss, I. Banyai, L. Iordanidis, T. Mavromoustakos, A. Salifoglou, Inorg. Chem. 40 (2001) 1734, and references therein.
[57] C.L. Edwards, R.L. Hayes, J. Am. Med. Assoc. 212 (1970) 1182.
[58] S. Jurisson, D. Berning, W. Jia, D. Ma, Chem. Rev. 93 (1993) 1137.
[59] P. Collery, C. Pechery, in: B. Keppler (Ed.), Metal Complexes in Cancer Chemotherapy, VCH, Weinheim, 1993, pp. 251–258.
[60] F. Kratz, B. Nuber, J. Weiss, B.K. Keppler, Polyhedron 11 (1992) 487.
[61] S. Zanias, C.P. Raptopoulou, A. Terzis, Th.F. Zafiropoulos, Inorg. Chem. Commun. 2 (1999) 48.
[62] G.S. Papaefstathiou, S. Manessi, C.P. Raptopoulou, E.J. Behrman, Th.F. Zafiropoulos, Inorg. Chem. Commun. 7 (2004) 69.
[63] G.M. Sheldrick, SHELXLS-86, Acta Crystallogr., Sect. A 46 (1990) 467.
[64] G.M. Sheldrick, SHELXL-93, Crystal Structure Refinement Program, University of Göttingen, Göttingen, Germany, 1993.
[65] H. Sigel, R.B. Martin, Chem. Rev. 82 (1982) 385.
[66] A. Sofetis, G.S. Papaefstathiou, A. Terzis, C.P. Raptopoulou, Th.F. Zafiropoulos, Z. Naturforsch. 59b (2004) 291.
[67] A.R. Barron, A.N. Maclnnes, in: R.B. King (Ed.), Encyclopedia of Inorganic Chemistry, vol. 3, Wiley, New York, 1994, pp. 1249–1269.
[68] R. Acevedo-Chávez, M.E. Costas, S. Bernès, G. Medina, L. Gasque, J. Chem. Soc., Dalton Trans. (2002) 2553.
[69] L.S. Gelfand, F.J. Iaconiani, L.L. Pytlewski, A.N. Speca, C.M. Mikulski, N.M. Karayannis, J. Inorg. Nucl. Chem. 42 (1980) 377.
[70] M. Tiliakos, E. Katsoulakou, V. Nastopoulos, A. Terzis, C. Raptopoulou, P. Cordopatis, E. Manessi-Zoupa, J. Inorg. Biochem. 93 (2003) 109, and references therein.
[71] R.J.H. Clark, C.S. Williams, Inorg. Chem. 4 (1965) 350.
[72] K. Nakamoto, Infrared and Raman Spectra of Inorganic and Coordination Compounds, fourth ed., Wiley, New York, 1986.